

## **Geophysical Research Letters**\*

## ب

#### RESEARCH LETTER

10.1029/2024GL109759

#### **Key Points:**

- Tree-ring series from ENSO rainfall impact regions reconstruct tropical Pacific SSTs with high degrees of skill back to 1500 CE and 1100 CE
- Two very different reconstruction methods produce similar results and each can only reconstruct the leading EOF mode of SST variability
- Reconstructions extending back 1100
  CE indicate a recent increase in El
  Niño variability, and overall SST
  warming in the equatorial Pacific

#### **Supporting Information:**

Supporting Information may be found in the online version of this article.

#### Correspondence to:

E. R. Cook, drdendro@ldeo.columbia.edu

#### Citation:

Cook, E. R., & Cane, M. A. (2024). Tree rings reveal ENSO in the last millennium. *Geophysical Research Letters*, 51, e2024GL109759. https://doi.org/10.1029/2024GL109759

Received 22 APR 2024 Accepted 5 SEP 2024

#### **Author Contributions:**

Conceptualization: Edward R. Cook
Data curation: Edward R. Cook
Formal analysis: Edward R. Cook, Mark
A. Cane
Methodology: Edward R. Cook, Mark
A. Cane

Software: Edward R. Cook Validation: Edward R. Cook, Mark A. Cane Writing – original draft: Edward

R. Cook, Mark A. Cane
Writing – review & editing: Mark

A. Cane

© 2024. The Author(s).
This is an open access article under the terms of the Creative Commons
Attribution License, which permits use, distribution and reproduction in any medium, provided the original work is properly cited.

## Tree Rings Reveal ENSO in the Last Millennium

Edward R. Cook<sup>1</sup> and Mark A. Cane<sup>1</sup>

<sup>1</sup>Lamont-Doherty Earth Observatory, Palisades, NY, USA

**Abstract** We present new climate field reconstructions (CFR) of tropical Pacific ENSO sea surface temperatures (HadISST) for the boreal winter season using a circum-Pacific tree-ring network from known El Niño rainfall impact regions. We use two different CFR methods: Point-by-Point Regression (PPR) and reduced-space Orthogonal Spatial Regression (OSR). Both methods produce reconstructions with high validation skill, but OSR is preferred because it has less spatial noise and is more efficient. Only the leading EOF of the SST field (EOF1) can be skillfully reconstructed by either method; EOF2 does not validate. The success of EOF1 reflects its importance for ENSO rainfall impacts over land; the failure with EOF2 is from the lack of these impacts. EOF1 allows for the reconstruction of many ENSO indices, including the ENSO Longitudinal Index (ELI). We also find evidence in our reconstructions for a recent increase in ENSO activity.

Plain Language Summary Earth's climate is strongly affected by how warm the tropical Pacific Ocean "El Niño" region is. This is especially true for the delivery of rainfall over many parts of the globe. Tree growth can thus be strongly affected by El Niño impacts on rainfall. We use this relationship to reconstruct tropical Pacific sea surface temperatures associated with El Niño over most of the past millennium from a network of annual tree-ring chronologies located in regions known to be impacted by El Niño rainfall. Only the leading mode of variability in Pacific sea surface temperatures associated with El Niño can be reconstructed well, but it reflects most of the long-term variability of El Niño exceptionally well. The reconstruction extends back to 1500 with exceptional skill and back to 1100 with acceptable skill. We can thus compare recent El Niño variability, perhaps affected by global warming, with what happened over the previous centuries unaffected by human activity. We find evidence for an increase in El Niño activity, and for an overall warming in recent decades.

#### 1. Introduction

The global importance of the El Niño Southern Oscillation (ENSO) is undisputed and extremely well researched both theoretically and empirically (e.g., McPhaden et al. (2020); Sarachik and Cane (2010) for comprehensive reviews of ENSO). The record of ENSO based on instrumental data extends back only to the mid-19th Century and since an El Niño event occurs roughly every 4 years on average, this record provides only ~40 cycles (e.g., Kaplan et al., 1998). These recurrences show great variability in frequency and amplitude from decade to decade, as well as differences in spatial pattern (Capotondi et al., 2015). The purpose of this paper is to develop a skillful gridded field reconstruction of tropical Pacific SSTs to extend the record of ENSO variability back in time to better characterize this variability.

An inescapable question is how ENSO will be affected by global warming. Though there is no firm consensus, the current leading hypothesis is that ENSO events will become stronger and more frequent in the future (e.g., Cai et al., 2018). This projection is based on Earth System Models (ESMs), the same models that have failed to match the observed record in the tropical Pacific since 1950, when the global warming signal begins to emerge from the natural background (e.g., Seager et al., 2019, 2022). Hence the need for paleoclimate estimates of ENSO variability.

This paper is about observations and does not mention ESMs again. We extend the record of ENSO back to 1500 CE with high skill and usefully so to 1100 CE by inferring the state of the tropical Pacific from ENSO sensitive tree ring records associated with regional rainfall impacts. We then use these SST field reconstructions to evaluate annual changes in ENSO variability, including that expressed by the ENSO Longitudinal Index (ELI; Williams & Patricola, 2018).

COOK AND CANE 1 of 9

#### 2. Data and Methods

We aim to skillfully reconstruct tropical Pacific sea surface temperatures (SSTs) from tree ring records over the past millennium. Accordingly, two types of data are used: (a) moisture-sensitive tree-ring records used for developing circum-Pacific drought atlases (Cook et al., 2004, 2010; Morales et al., 2020; Palmer et al., 2015; Stahle et al., 2016); (b) SSTs in the tropical Pacific region of (10N–10S, 80W–160E) from the 1° × 1° HadISST analysis (Rayner et al., 2003; HAD) beginning in 1870. To address the common problem of overfitting statistical models we restrict our candidate pool of tree-ring predictors to locations where ENSO has known impacts on rainfall (Lenssen et al., 2020; Figure S1A in Supporting Information S1). We then reduce this large pool from 1757 to 544 chronologies by statistical screening as described in Methods of the Supporting Information S1. The remaining 544 screened chronologies begin on or before 1800 and diminish to 81 by 1100.

We target only the boreal winter (DJF) season SST, when ENSO has the strongest effect on global climate. To calibrate our reconstructions, we use SST data from 1930 through 2000; data from 1871 to 1929 are withheld to validate the tree-ring estimates. Extensive validation testing of our SST reconstructions using rigorous tests like Coefficient of Efficiency (CE) (Briffa et al., 1988) indicate that they have high levels of skill (Figure S4, Table S1 in Supporting Information S1). We also check results against other SST data sets derived from instrumental records (ERSST5, Huang et al., 2017; KAP, Kaplan et al., 1998) and find no substantive changes in validation skill (Table S2 in Supporting Information S1).

We regress the target SSTs on the tree ring data using two different climate field reconstruction methods. PPR (Point by Point Regression; Cook et al., 1999) individually predicts the SST in each of the 2,397 1° × 1° grid boxes in the target domain. The other, OSR (Orthogonal Spatial Regression; Briffa et al., 1986; Cook et al., 1994), first rotates the SST data over the calibration period into a set of EOFs and individually predicts the principal component (PC) associated with each EOF. Individual grid point SSTs are obtained by back-transforming from EOF space to SST space. Since there can be no more than 71 EOFs from data spanning 1930–2000, and far fewer account for most of the variance, OSR will involve many fewer individual predictions than PPR. An open question is what more, if anything, may be recovered by the more computationally intensive PPR method. For OSR, we base the EOFs on the correlation matrix of the HAD grid points rather than the covariance matrix in order to give more weight to warmer points, which typically have less variance but more influence on teleconnected impacts because greater atmospheric convection tends over warmer waters (Sarachik & Cane, 2010). Results using covariance-based EOFs do not differ greatly (not shown).

In order to fully use the longer tree-ring chronologies available for reconstruction, and thus produce the longest well-validated ENSO field reconstruction possible, PPR and OSR are applied multiple times in a stepwise "nested" fashion to allow each reconstruction to be extended back in time as shorter tree-ring chronologies became unavailable. For both PPR and OSR the starting year of each reconstruction nest (tree rings over a fixed common interval) steps back at 100 years intervals, beginning in 1800 and extending back to 1100 CE, with the calibration and validation skill of each new model individually evaluated. We label these reconstructions R18, R17, ... R11. Prior to 1100 the reconstruction does not validate due to the loss of ENSO-sensitive chronologies from Southeast Asia (Buckley et al., 2017; Figure S4 in Supporting Information S1).

#### 2.1. OSR Versus PPR Methods of Reconstruction

As a reduced-space method, OSR reconstructs only a limited number of EOFs. Here we reconstruct the three leading HAD EOFs selected by the "North test" (North et al., 1982; Figure S2 in Supporting Information S1), which cumulatively account for 88.4% of the total field variance. Taking HAD as "truth," Figure 1a shows maps of the OSR and PPR calibration and validation statistics using tree-ring chronologies available from 1800 (R18). Both methods have high skill except at the western end of the domain, and, for validation, at the southeast, but OSR skill is high over a larger area. OSR also shows less small-scale variability, a benefit of spatial smoothing. Overall, Figure 1 shows that OSR performs slightly better than PPR; the far greater computational burden of PPR has failed to add desirable features.

The PPR method does not use the spatial correlations within the domain for reconstruction. Thus, how well does it recover them? To determine that we examine the EOFs and associated PCs of the HAD, OSR, and PPR fields over 1871–2000. By construction, OSR EOFs are very similar to HAD EOFs (Figure S3 in Supporting Information S1). PPR, which is not constrained a priori to approximate the HAD EOFs is, nonetheless, similar to HAD.

COOK AND CANE 2 of 9

elibrary.wiley.com/doi/10.1029/2024GL109759 by Columbia University Libraries, Wiley Online Library on [16/10/2024]. See the Terms and Conditions

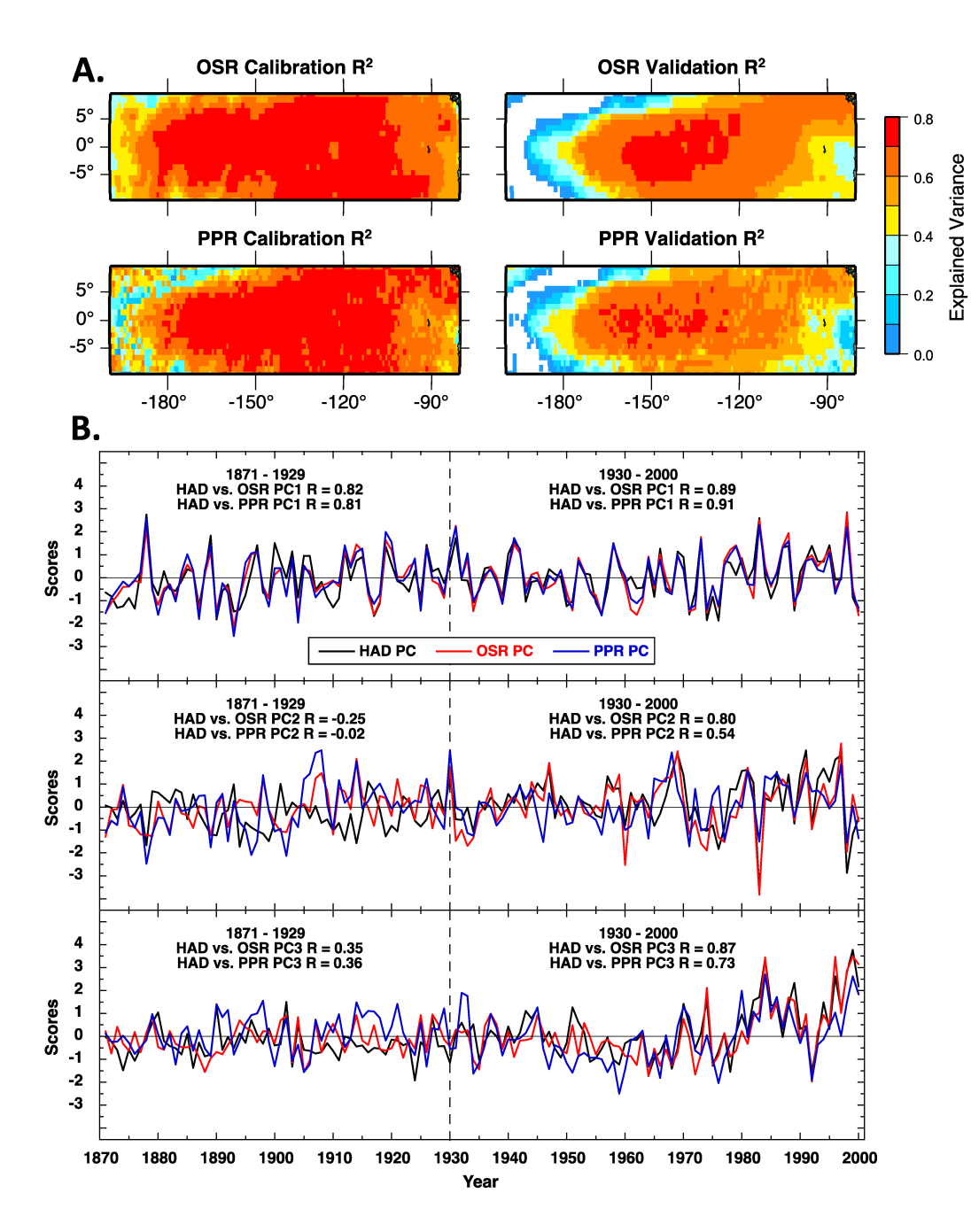


**Figure 1.** Top (a) shows maps of the OSR and PPR calibration and validation statistics for the R18 tree-ring chronology nest. The bottom plots (b) compare the three principal components (PC1, PC2, PC3) of the EOFs reconstructed by OSR and PPR with the PCs of HAD over the calibration (1930–2000) and the validation (1871–1929) periods.

For HAD and OSR the leading three EOFs are well separated based on the North test (Figure S2 in Supporting Information S1). For the PPR method only the first EOF is distinct.

Figure 1b compares the corresponding three PCs from the OSR and PPR reconstructions with the PCs of HAD over the calibration (1930–2000) and validation (1871–1929) periods. PC1 from either is very highly correlated with HAD PC1 for both the calibration period (OSR R = 0.90, PPR R = 0.91) and the validation period (OSR R = 0.82, PPR R = 0.81). PC2 (OSR R = 0.80, PPR R = 0.54) and PC3 (OSR R = 0.87, PPR R = 0.73) calibration period correlations are also high, but the validation correlations are negative for PC2 (OSR R = -0.25, PPR R = -0.02) and weak for PC3 (OSR R = 0.35, PPR R = 0.36). Experiments with other ways of selecting

COOK AND CANE 3 of 9

# Spearman correlations of CRU JFMA rainfall (1901-2000) with HAD, OSR, and PPR PC1 and PC2

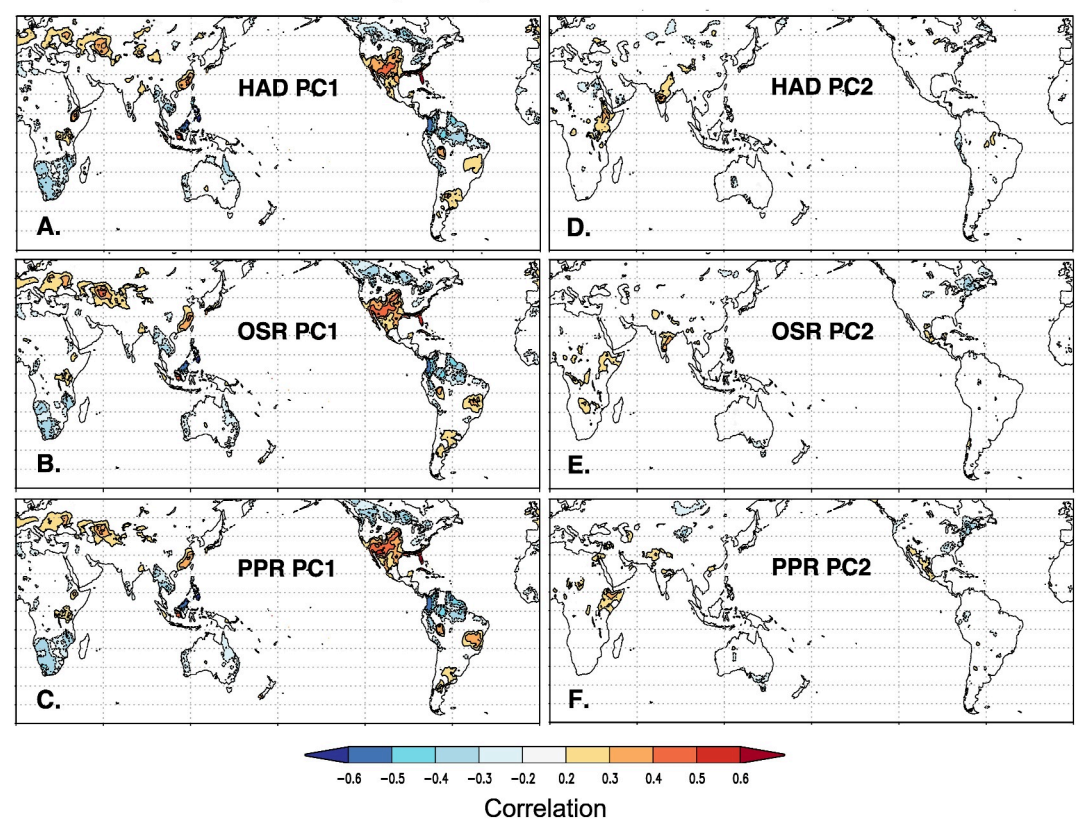


Figure 2. Rainfall correlations with HAD, OSR, and PPR PC1 (a–c) and PC2 (d–f) using Climatic Research Unit (CRU) rainfall data available at KNMI Climate Explorer (https://climexp.knmi.nl). Only PC1 has strong correlations with rainfall where the trees used for reconstruction are located. In contrast, PC2 has very little correlation with rainfall globally.

predictors did not improve validation skill. Both reconstruction methods overfit their calibration estimates of PC2 and PC3. In summary, OSR and PPR each do an excellent job of reconstructing PC1 from tree rings, but only PC1.

It may be that our reconstruction methodologies have contributed to the failure to capture more than PC1. However, the predictors we use are not in situ in the tropical Pacific, but rely on rainfall impacts distant from this target region. The tropical Pacific influences are likely to be large scale and not subtle, so it is plausible that only a single pattern, one most representative of ENSO, can be recovered by inverting ENSO's influence on tree growth. Figure 2 supports this idea. HAD, OSR, and PPR PC1 (2A-C) are connected to rainfall in many parts of the world where we have tree-ring chronologies (Figure S1 in Supporting Information S1). In contrast, PC2 (2D-F) has little connection to rainfall except weakly in central Africa where there are no tree ring chronologies in our models. This lack of correlation holds for the HAD instrumental data as well. We conclude that only PC1 can be reconstructed from our moisture sensitive tree-ring records. We also settle on OSR as our reconstruction method because it produces less spatial noise and is far less computationally demanding. All reconstruction results reported here from this point on are based on OSR.

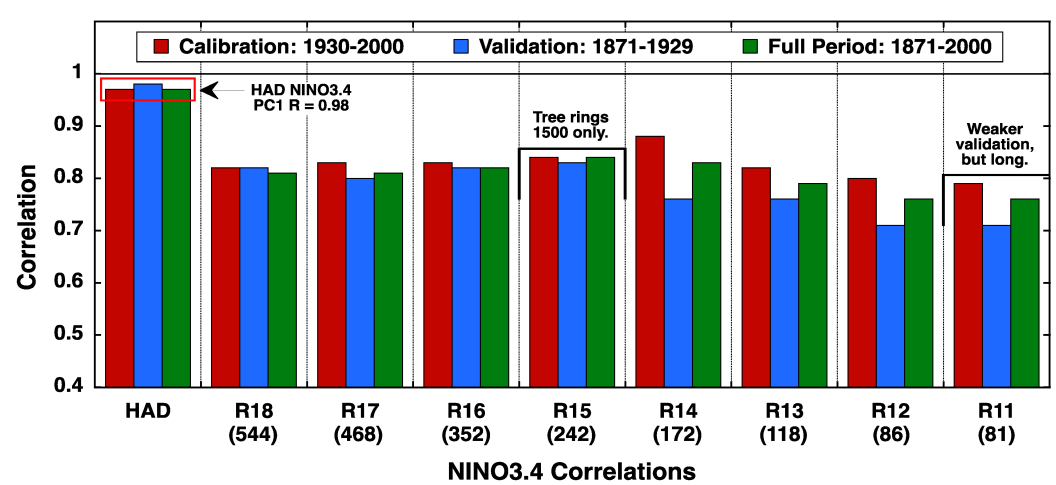
Figure 3a shows the calibration, validation and overall skill of OSR PC1 field reconstructions of HAD NINO3.4 using trees available (numbers in parentheses) for R18, R17, ... R11. See Figure S4 in Supporting Information S1 for a more detailed examinations of ENSO reconstruction skill at the grid point level. Figure 3 also shows the correlation of HAD NINO3.4 with HAD PC1 itself. It is 0.98 even for the validation period; that is, PC1 and NINO3.4 are effectively the same. There is also little change in skill among the reconstructions back to 1500. The highest R (0.83 for the validation period) is for the R15 reconstruction and there is little difference in skill between its calibration and validation periods, indicating that the calibration model is not overfit. Before 1500 skill

COOK AND CANE 4 of 9

19448007, 2024, 19, Downloaded

from https://agupubs.onlinelibrary.wiley.com/doi/10.1029/2024GL109759 by Columbia University Libraries, Wiley Online Library on [16/10/2024]. See the Terms and Condit





#### B. HAD PC1 & R15 PC1 vs. ENSO Indices

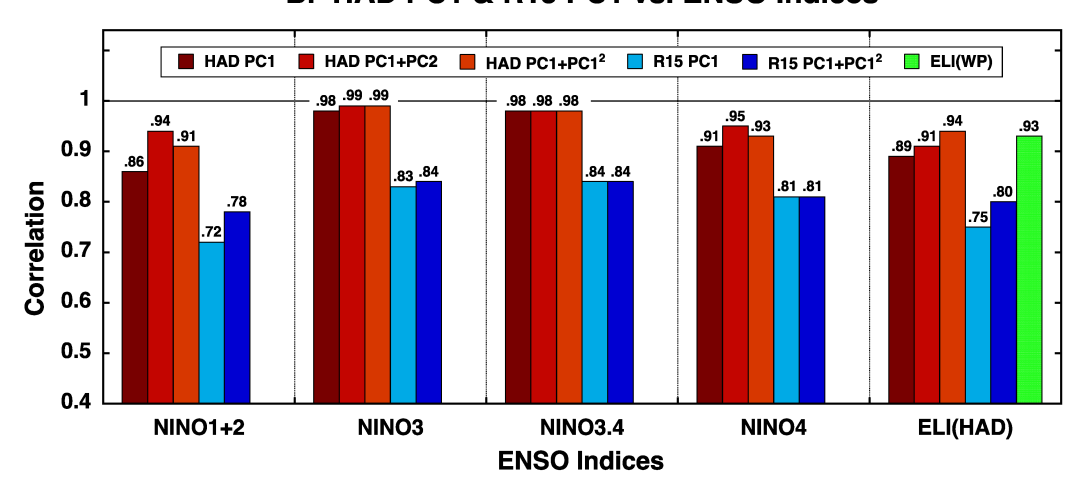


**Figure 3.** Top bar plot (a) shows the calibration, validation and overall skill of reconstructions of HAD NINO3.4 using PC1 from HAD and the reconstructions based on trees available (in parentheses) in the common period nests. R15 is the best by a small margin. The bottom bar plot (b) shows how well HAD PC1 and R15 PC1 reconstruct various ENSO indices (1871–2000). We also correlate our estimate of the ELI from HAD with ELI from Williams and Patricola (2018).

decreases and validation skill is less then calibration skill. Nonetheless, the reconstruction back to 1100 accounts for 50% of the validation period variance, which is still useful. The R15 and R11 reconstructions are further validated against ERSST and KAP SST data (Table S2 in Supporting Information S1) and the results are consistent with what is reported in Figure 3.

Figure 3b displays correlations of various common ENSO indices from HAD or R15. In addition to those based on PC1 only, regressions on PC1 plus PC1 $^2$  allow for possible missing nonlinear relationships. For HAD we also do regressions on PC1 plus PC2 to see what is lost by the reconstructions not having PC2. HAD PC1 accounts for effectively all NINO3 and NINO3.4 variance; PC1 is essentially interchangeable with these indices. Thus, nothing is gained by including PC2 or PC1 $^2$  in the regression. NINO1+2 and NINO4 are slightly improved by including PC2, and adding PC1 $^2$  to PC1 is almost as good. With R15 PC1 the correlations for NINO3, NINO3.4 and NINO4 are above 0.8 and little is gained by adding PC1 $^2$ , but for NINO1+2 the correlation is improved from 0.72 to 0.78 by adding PC1 $^2$ , compensating for the absence of PC2 in the R15 reconstruction. We also include a correlation between an estimate of the ELI from our HAD DJF target field with DJF ELI available from Williams and Patricola (2018), the latter based on ERSST data. The correlation (R = 0.93) is extremely high.

COOK AND CANE 5 of 9

from https://agupubs.onlinelibrary.wiley.com/doi/10.1029/2024GL109759 by Columbia University Libraries, Wiley Online Library on [16/10/2024]

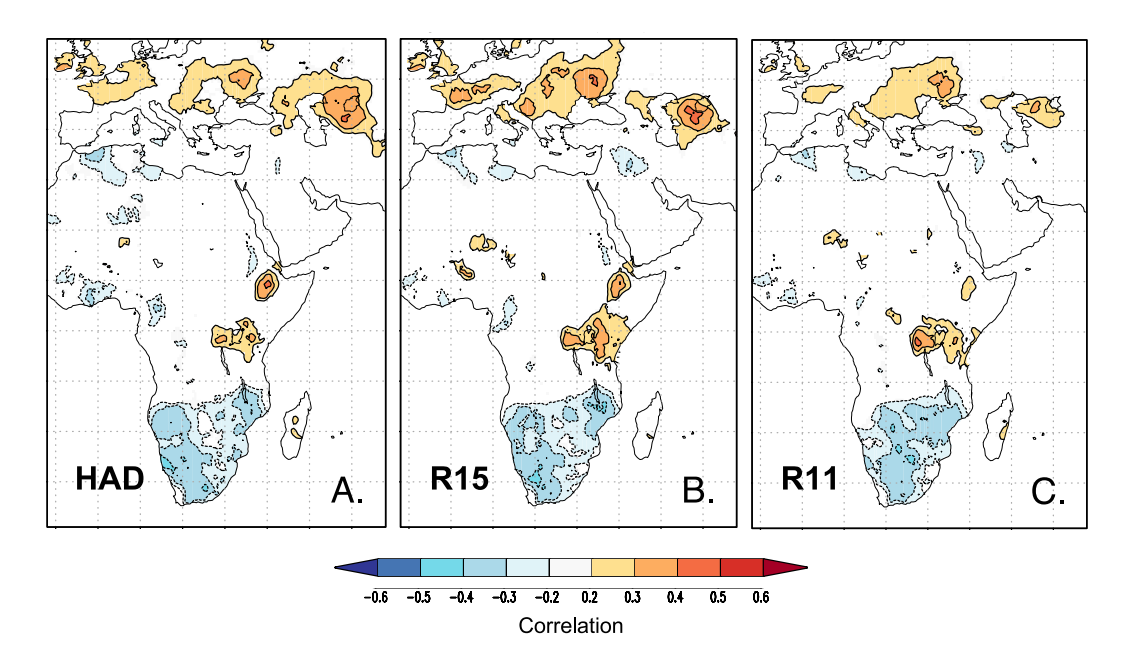


**Figure 4.** Rainfall correlations over Africa, Europe, and the Middle East from HAD (a), R15 (b), and R11 (c) PC1s based on reconstructing SST EOF1. The pattern in the R15 panel is almost indistinguishable from that in the HAD panel. R11, with less skill, is nearly as good.

Global correlations of rainfall with R15 and R11 PC1 testifies to the skill of these reconstructions. The correlation patterns for R15 and R11 (Figure S5 in Supporting Information S1) are very similar to that for HAD and also very similar to the PC1 rainfall correlation maps shown in Figure 2. However, this is not an entirely independent test, as much of the rainfall field overlaps geographically with the trees used in the reconstructions. In contrast, rainfall correlations over Africa, Europe, and the Middle East from HAD (A), R15 (B), and R11 (C) PC1s (Figure 4) provide a true out-of-sample comparison because no tree-ring chronologies in the area shown were used in the reconstructions. The pattern in the R15 panel is almost indistinguishable from that in the HAD panel. R11, a reconstruction with less skill, is still close to the other two in capturing this ENSO impact on rainfall. These findings are consistent with comparisons of NINO3.4 indices estimated from CRU and GPCC teleconnected precipitation data (van Oldenborgh et al., 2021) with HAD, R15, and R11 PC1 (Figure S6 in Supporting Information S1). R15 has correlations >0.8 with GPCC and CRU NINO3.4 indices, which are almost the same as those for HAD. R11 correlations are lower, but still highly significant.

The final ENSO index investigated here is the ELI (ENSO Longitudinal Index) of Williams and Patricola (2018; WP). It is a continuous measure intended to capture ENSO diversity related to the mean longitude of deep convection each year. WP ELI has a strong quadratic relationship with HAD, R15, and R11 PC1s (Figure 3b; Figure S7 in Supporting Information S1). This could be anticipated in view of the relation between ELI and NINO3 shown in WP (their Figure S6). Given these strong relationships, we regressed our R15 and R11 PCs on WP ELI to produce our own reconstructions of ELI back to 1500 and 1100 (Figure 5; Figure S7 in Supporting Information S1).

Figures 5a and 5b suggests overall warming, greater variability, and an eastward shift in the ELI has occurred in recent decades. Wavelet power spectra (Figure S8 in Supporting Information S1) also suggest that the amplitude of ENSO variability centered at ~4 years has increased. To further investigate this observation, we calculated 20-year running means of average amplitude and its standard deviation. Timeseries shown in Figure S9 of the Supporting Information S1 and their distributions in Figure S10 of the Supporting Information S1 support the finding that the warmest temperatures and strongest variability since 1600 have occurred in the decades since 1960. However, periods almost as warm and variable are also found around 1700 and 1800. We note that warmer temperatures are not always associated with greater variability (viz. Figure S9 in Supporting Information S1). The rank correlation between the two in the R15 record is only 0.34.

COOK AND CANE 6 of 9

19448007, 2024, 19, Downl

from https://agupubs.onlinelibrary.wiley.com/doi/10.1029/2024GL109759 by Columbia University Libraries, Wiley Online Library on [16/10/2024].

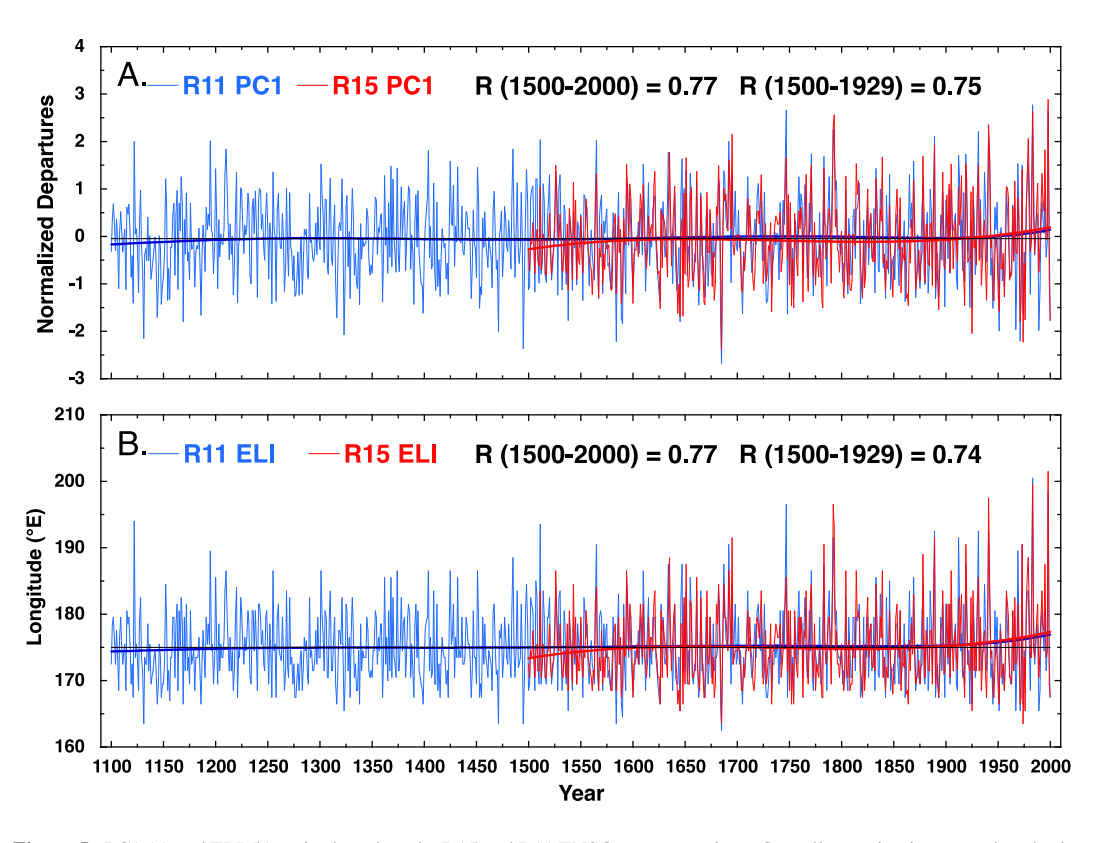


**Figure 5.** PC1 (a) and ELI (b) series based on the R15 and R11 ENSO reconstructions. Overall warming in recent decades is indicated by smooth polynomial curves. Full overlap and pre-calibration correlations are shown.

#### 3. Summary and Discussion

We began this work with a number of questions. The overarching one was how skillfully can we reconstruct DJF tropical Pacific (ENSO) SST fields from *remote impacts* on moisture sensitive trees without any in situ data from the tropical Pacific? While this has been done several times before for ENSO indices (e.g., D'Arrigo et al., 2005; Li et al., 2013; Stahle et al., 1998; Wilson et al., 2010), we have taken an intensive new look at it as a spatial reconstruction problem, with emphasis placed on restricting our tree-ring series used for reconstruction to areas of known ENSO impact on rainfall (Lenssen et al., 2020; Figure S1 in Supporting Information S1), and to extensive validation testing of our estimates (Figure S4, Tables S1 and S2 in Supporting Information S1). We used two different reconstruction methods: PPR uses the tree-ring chronologies to estimate each of the 2,397 1° × 1° SST boxes in our target area while OSR targets the leading EOFs of the SST field. Would PPR provide more information about the target SST field? It turned out that they have roughly equivalent skill (Figure 1a). We settled on OSR because its reconstructions are somewhat less noisy and is far less computationally demanding.

The next question is how many SST EOFs/PCs can we reconstruct? The answer is: just one, the leading mode (Figure 1b). The inability to skillfully estimate PC2 from moisture sensitive trees is shown to be due to the lack of any connection between rainfall and PC2 of tropical Pacific SST (Figures 2d–2f). Disappointing perhaps, but the reconstruction of PC1 is exceptionally skillful. Moreover, the leading mode accounts for almost 72% of the original SST field variance. Fortunately, PC1 is sufficient to allow excellent estimates of some common ENSO indices (NINO3, NINO3.4) and good estimates of others (NINO4, NINO1+2); see Figure 3b and Table S2 in Supporting Information S1. The nonlinear ELI is also well captured by a quadratic function of PC1 (Figure S7 in Supporting Information S1).

How far back in time can we go with useful skill? We found little difference in skill between using all 544 chronologies from 1800 CE and using fewer than half as many (242) available back to 1500 CE (Figure 3a, Figure S4 in Supporting Information S1). Over the validation period (1871–1929) the correlation of the instrumental HAD PC1 with this R15 reconstruction is R = 0.83, accounting for almost 70% of the variance, making it one of

COOK AND CANE 7 of 9

the most skillful proxy reconstructions we know of (see Table S1 in Supporting Information S1). This out-of-calibration skill is only slightly lower than the R = 0.84 for the calibration period (1930–2000), indicating that there is little overfitting. With only the 81 chronologies going back to 1100 CE the validation period correlation of R11 PC1 with HAD PC1 is 0.71, still high enough to be useful. The higher R (0.79) in the calibration period is indicative of some overfitting.

A virtue of our reconstructions is the precision of tree-ring dating. All banded annual proxies—tree rings, ice cores, corals, speleothems, lake sediments—are subject to dating errors. Annual bands can be missing or missed, and intra-annual features can be counted as annual bands. Dendrochronologists address this by replication within each chronology, which enables rigorous crossdating (Fritts, 1976). Moreover, many tree-ring chronologies go into our estimates of ENSO PC1 making it virtually certain that the annual dating of our reconstructions is correct. Replication is more difficult with other proxies, but has been done for some, like corals (DeLong et al., 2007; Hendy et al., 2003; Lough, 2004).

Our reconstructions rely on remote impacts of tropical Pacific SST on rainfall. No in situ ENSO proxies are used; only trees that record these impacts very well. We speculate that our indices are consequently robust indicators of ENSO impacts, possibly as good or better than NINO3.4 or some other SST measure for this purpose. Their relation to rainfall shown in Figures 2 and 4 support this speculation, but how broadly it holds is unknown.

Figures 5a and 5b show the R11 and R15 reconstructions of PC1 (equivalently, NINO3.4) and the ENSO Longitudinal Index (ELI) based on regression (Figure S7 in Supporting Information S1) back in time with smooth polynomial curves applied to highlight recent warming. The positive excursions (i.e., El Niño events) in recent decades are generally higher than at any time since 1100. Further investigation of the more skillful R15 record (Figures S9 and S10 in Supporting Information S1) shows that the recent decades have higher ENSO variability than at any time since 1600. Episodes of greater variability in the past are not always accompanied by warmer temperatures, and it may be that the recent increase is more related to the stronger zonal gradient in the equatorial Pacific (Seager et al., 2019) rather than warming per se. But the world is warmer, and these impact-based indices suggest that the impacts are becoming more severe.

#### **Conflict of Interest**

The authors declare no conflicts of interest relevant to this study.

#### **Data Availability Statement**

The Hadley Centre Sea Ice and Sea Surface Temperature data set (HadISST) is available from https://www.metoffice.gov.uk/hadobs/hadisst/. The HadISST target field data, along with the R15 and R11 reconstructed HadISST fields, are available at NOAA-NCEI Paleoclimatology (Cook & Cane, 2024).

#### References

Briffa, K. R., Jones, P. D., Pilcher, J. R., & Hughes, M. K. (1988). Reconstructing summer temperatures in northern Fennoscandinavia back to A. D. 1700 using tree-ring data from Scots pine. Arctic and Alpine Research, 20(4), 385–394. https://doi.org/10.2307/1551336

Briffa, K. R., Jones, P. D., Wigley, T. M. L., Pilcher, J. R., & Baillie, M. G. L. (1986). Climate reconstruction from tree rings: Part 2, spatial reconstruction of summer mean sea-level pressure patterns over Great Britain. *Journal of Climatology*, 6, 1–15. https://doi.org/10.1002/joc. 3370060102

Buckley, B. M., Stahle, D. K., Luu, H. T., Wang, S.-Y., Nguyen, T., Thomas, P., et al. (2017). Central Vietnam climate over the past five centuries from cypress tree rings. Climate Dynamics, 48(11–12), 3707–3723. https://doi.org/10.1007/s00382-016-3297-y

Cai, W., Wang, G., Dewitte, B., Wu, L., Santoso, A., Takahashi, K., et al. (2018). Increased variability of eastern Pacific El Niño under greenhouse warming. *Nature*, 564(7735), 201–206. https://doi.org/10.1038/s41586-018-0776-9

Capotondi, A., Wittenberg, A. T., Newman, M., Di Lorenzo, E., Yu, J.-Y., Braconnot, P., et al. (2015). Understanding ENSO diversity. Bulletin of the American Meteorological Society, 96(6), 921–938. https://doi.org/10.1175/BAMS-D-13-00117.1

Cook, E. R., Anchukaitis, K. J., Buckley, B. M., D'Arrigo, R. D., Jacoby, G. C., & Wright, W. E. (2010). Asian monsoon failure and megadrought during the last millennium. Science, 328(5977), 486–489. https://doi.org/10.1126/science.1185188

Cook, E. R., Briffa, K. R., & Jones, P. D. (1994). Spatial regression methods in dendroclimatology: A review and comparison of two techniques. International Journal of Climatology, 14(4), 379–402. https://doi.org/10.1002/joc.3370140404

Cook, E. R., & Cane, M. A. (2024). NOAA/WDS paleoclimatology—Equatorial Pacific tree ring based SST reconstruction 1100-2000 CE [Dataset]. NOAA National Centers for Environmental Information. https://doi.org/10.25921/1hke-2d71

Cook, E. R., Meko, D. M., Stahle, D. W., & Cleaveland, M. K. (1999). Drought reconstructions for the continental United States. *Journal of Climate*, 12(4), 1145–1162. https://doi.org/10.1175/1520-0442(1999)012<1145:DRFTCU>2.0.CO;2

Cook, E. R., Woodhouse, C., Eakin, C. M., Meko, D. M., & Stahle, D. W. (2004). Long-term aridity changes in the western United States. *Science*, 306(5698), 1015–1018. https://doi.org/10.1126/science.1102586

#### Acknowledgments

E. R. Cook and M. A. Cane acknowledge support of this research by the NSF Paleo Perspectives on Climate Change (P2C2) Program, Grant AGS 20-02452 (lead P.I. A. Kaplan). ERC was responsible for producing the reconstructions and both ERC and MAC for the analyses and interpretations presented. We thank J. Smerdon for producing the wavelet power spectra.

COOK AND CANE 8 of 9



### **Geophysical Research Letters**

- 10.1029/2024GL109759
- D'Arrigo, R., Cook, E. R., Wilson, R. J., Allan, R., & Mann, M. E. (2005). On the variability of ENSO over the past six centuries. *Geophysical Research Letters*, 32(3), L03711. https://doi.org/10.1029/2004GL022055
- DeLong, K. L., Quinn, T. M., & Taylor, F. W. (2007). Reconstructing twentieth-century sea surface temperature variability in the southwest Pacific: A replication study using multiple coral Sr/Ca records from New Caledonia. *Paleoceanography and Paleoclimatology*, 22(4), PA4212. https://doi.org/10.1029/2007PA001444
- Fritts, H. C. (1976). Tree rings and climate (p. 567). Academic Press.
- Hendy, E. J., Gagan, M., & Lough, J. M. (2003). Chronological control of coral records using luminescent lines and evidence for non-stationary ENSO teleconnections in northeast Australia. The Holocene, 13(2), 187–199. https://doi.org/10.1191/0959683603hl606rp
- Huang, B., Thorne, P., Banzon, V., Boyer, T., Chepurin, G., Lawrimore, J., et al. (2017). Extended reconstructed sea surface temperature, version 5 (ERSSTv5): Upgrades, validations, and intercomparisons. *Journal of Climate*, 30(20), 8179–8205. https://doi.org/10.1175/jcli-d-16-0836.1
- Kaplan, A., Cane, M. A., Kushnir, Y., Clement, A. C., Blumenthal, M. B., & Rajagopalan, B. (1998). Analyses of global sea surface temperature 1856–1991. *Journal of Geophysical Research*, 103(C9), 18567–18589. https://doi.org/10.1029/97JC01736
- Lenssen, N. J. L., Goddard, L., & Mason, S. (2020). Seasonal forecast skill of ENSO teleconnection maps. Weather and Forecasting, 35(6), 2387–2406. https://doi.org/10.1175/WAF-D-19-0235.1
- Li, J., Xie, S.-P., Cook, E., Morales, M., Christie, D., Johnson, N. C., et al. (2013). El Niño modulations over the past seven centuries. *Nature Climate Change*, 3(9), 822–826. https://doi.org/10.1038/nclimate1936
- Lough, J. M. (2004). A strategy to improve the contribution of coral data to high-resolution paleoclimatology. Palaeogeography, Palaeoclimatology, Palaeoecology, 204(1-2), 115–143. https://doi.org/10.1016/s0031-0182(03)00727-2
- M. McPhaden, A. Santoso, & W. Cai (Eds.) (2020). El Niño Southern Oscillation in a changing climate. https://doi.org/10.1002/9781119548164
  Morales, M. S., Cook, E. R., Barichivich, J., Christie, D. A., Villalba, R., LeQuesne, C., et al. (2020). Six hundred years of South American tree rings reveal an increase in severe hydroclimatic events since mid-20th century. Proceedings of the National Academy Sciences of the United States of America, 117(29), 16816–16823. https://doi.org/10.1073/pnas.2002411117
- North, G. R., Bell, T. L., & Cahalan, R. (1982). Sampling errors in the estimation of empirical orthogonal functions. *Monthly Weather Review*, 110(7), 699–706. https://doi.org/10.1175/1520-0493(1982)110%3C0699:SEITEO%3E2.0.CO;2
- Palmer, J. G., Cook, E., Turney, C., Allen, K., Fenwick, P., Cook, B., et al. (2015). Drought variability in the eastern Australia and New Zealand summer drought atlas (ANZDA, CE 1500-2012) modulated by the Interdecadal Pacific Oscillation. *Environmental Research Letters*, 10(12), 124002. https://doi.org/10.1088/1748-9326/10/12/124002
- Rayner, N. A., Parker, D. E., Horton, E. B., Folland, C. K., Alexander, L. V., Rowell, D. P., et al. (2003). Global analyses of sea surface temperature, sea ice, and night marine air temperature since the late nineteenth century. *Journal of Geophysical Research*, 108(D14), 4407. https://doi.org/10.1029/2002JD002670
- Sarachik, E., & Cane, M. (2010). The El Niño-Southern Oscillation phenomenon. Cambridge University Press. Retrieved from https://www.cambridge.org/core/books/el-ninosouthern-oscillation-phenomenon/DBB063CB79D4E97350B09F16B8A156A1
- Seager, R., Cane, M., Henderson, N., Lee, D.-E., Abernathey, R., & Zhang, H. (2019). Strengthening tropical Pacific zonal sea surface temperature gradient consistent with rising greenhouse gases. *Nature Climate Change*, 9(7), 517–522. https://doi.org/10.1038/s41558-019-0505-x
- Seager, R., Henderson, N., & Cane, M. (2022). Persistent discrepancies between observed and modeled trends in the tropical Pacific Ocean. Journal of Climate, 35(14), 4571–4584. https://doi.org/10.1175/jcli-d-21-0648.1
- Stahle, D. W., Cook, E. R., Burnette, D. J., Villanueva, J., Cerano, J., Burns, J. N., et al. (2016). The Mexican drought atlas: Tree-ring reconstructions of the soil moisture balance during the last pre-Hispanic, colonial, and modern eras. *Quaternary Science Reviews*, 149, 34–60. https://doi.org/10.1016/j.quascirev.2016.06.018
- Stahle, D. W., D'Arrigo, R. D., Krusic, P. J., Cleaveland, M. K., Cook, E. R., Allan, R. J., et al. (1998). Experimental dendroclimatic reconstruction of the Southern Oscillation. *Bulletin of the American Meteorological Society*, 79(10), 2137–2152. https://doi.org/10.1175/1520-0477 (1998)079<2137:edrots>2.0.co:2
- van Oldenborgh, G. J., Hendon, H., Stockdale, T., L'Heureux, M., Coughlan de Perez, E., Singh, R., & Aalst, M. (2021). Defining El Niño indices in a warming climate. *Environmental Research Letters*, 16(4), 044003. https://doi.org/10.1088/1748-9326/abe9ed
- Williams, I. N., & Patricola, C. M. (2018). Diversity of ENSO events unified by convective threshold sea surface temperature: A nonlinear ENSO index. Geophysical Research Letters, 45(17), 9236–9244. https://doi.org/10.1029/2018GL079203
- Wilson, R., Cook, E., D'Arrigo, R., Riedwyl, N., Evans, M., Tudhope, A. W., & Allan, R. (2010). Reconstructing ENSO: The influence of method, proxy data, climate forcing and teleconnections. *Journal of Quaternary Science*, 25(1), 62–78. https://doi.org/10.1002/jqs.1297

#### **References From the Supporting Information**

- Christiansen, D. E. (2012). Simulation of daily streamflows at gaged and ungaged locations within the Cedar River Basin, Iowa, using a precipitation-runoff modeling system model (p. 20). U.S. Geological Survey Scientific Investigations Report 2012–5213.
- Dawdy, D. R., & Matalas, N. C. (1964). In V. T. Chow (Ed.), Handbook of applied hydrology (p. 87). McGraw-Hill.
- Efron, B. (1987). Better bootstrap confidence intervals. *Journal of the American Statistical Association*, 82(397), 171–185. https://doi.org/10.1080/01621459.1987.10478410
- Furtado, J. C., Di Lorenzo, E., Cobb, K. M., & Bracco, A. (2009). Paleoclimate reconstructions of tropical sea surface temperatures from precipitation proxies: Methods, uncertainties, and nonstationarity. *Journal of Climate*, 22(5), 1104–1123. https://doi.org/10.1175/2008jcli2415.1
- Luo, X., Dee, S., Stevenson, S., Okumura, Y., Steiger, N., & Parsons, L. (2022). Last millennium ENSO diversity and North American tele-connections: New insights from paleoclimate data assimilation. *Paleoceanography and Paleoclimatology*, 37(3), e2021PA004283. https://doi.org/10.1029/2021PA004283
- Meko, D. M. (1981). Applications of Box-Jenkins methods of time series analysis to the reconstruction of drought from tree rings. Unpublished Ph.D. Dissertation (p. 149). The University of Arizona.
- Moriasi, D. N., Gitau, M. W., Pai, N., & Daggupati, P. (2015). Hydrologic and water quality models: Performance measures and evaluation criteria. *Transactions of the ASABE*, 58, 1763–1785.
- Nash, J. E., & Sutcliffe, J. V. (1971). River flow forecasting through conceptual models part I—A discussion of principles. *Journal of Hydrology*, 10(3), 282–290. https://doi.org/10.1016/0022-1694(70)90255-6
- Torrence, C., & Compo, G. P. (1998). A practical guide to wavelet analysis. Bulletin of the American Meteorological Society, 79(1), 61–78. https://doi.org/10.1175/1520-0477(1998)079<0061:APGTWA>2.0.CO;2
- Wahl, E. R., & Smerdon, J. E. (2012). Comparative performance of paleoclimate field and index reconstructions derived from climate proxies and noise-only predictors. *Geophysical Research Letters*, 39(6), L06703. https://doi.org/10.1029/2012GL051086

COOK AND CANE 9 of 9